

HIGH-FIDELITY FINITE ELEMENT MODELLING OF MASS-TIMBER MEMBERS SUBJECTED TO SIMULATED FAR-FIELD BLAST LOADS

Mehdi Saloo¹, Christian Viau², Ghasan Doudak³

ABSTRACT: This paper presents a numerical study using the finite element (FE) method through LS-DYNA investigating the behaviour of glued laminated timber (glulam) beams and cross-laminated timber (CLT) panels subjected to shock-tube simulated blast loads. The modeling approach is validated with experimental shock-tube test results. The study shows that the FE models capture the overall failure modes and damage extent for glulam and CLT members with reasonable accuracy. Additionally, high-fidelity modelling shows the potential to accurately predict the dynamic behaviour of heavy timber elements in terms of displacement-time history and resistance curves, which is important for designing safer timber structures subjected to far-field blast loads.

KEYWORDS: Blast loads, timber, glulam, cross-laminated timber, LS-DYNA, finite element analysis

1 – INTRODUCTION

Recent experimental studies investigating timber elements and connections subjected to blast loads [e.g., 1-8] have in part contributed to the development of the Canadian blast standard, CSA S850 [9]. These studies involved the use of a shock tube test facility, which simulates the effects of far-field blast loads through a double-diaphragm firing system, without the need for live explosives testing. Additionally, simplified analysis methods using single-degree-of-freedom (SDOF) modelling have been investigated and found to accurately predict the overall behaviour of individual elements until the point of ultimate failure. However, while these models can capture the global response of timber elements beyond initial failure, they lack the resolution to accurately predict detailed phenomena such as crack initiation, propagation, internal stress distributions, and the extent of damage within the members. While experimental testing and simplified analytical methods have been successfully used to study overall behaviour of timber elements, FE modelling has become an increasingly valuable tool due to its numerous advantages. FE modelling allows for detailed simulation of complex behaviours, such as wood's anisotropic and heterogeneous nature. It also provides flexibility in quickly and effectively evaluating multiple failure modes, load conditions, and design configurations. Despite these advantages, limited studies involving numerical modelling

have been conducted for dynamically loaded timber elements, mainly due to the challenges associated with accurately defining wood's material properties and complex failure mechanisms. This gap underscores the significance of this study, which aims to contribute to developing more accurate FE models for timber structures. Oliveira, et al. [10] developed a FE model using the ABAQUS explicit solver [11], whereby the model could accurately predict the failure mode, crack propagation, and resistance curve of both glued-laminated timber (glulam) and cross-laminated timber (CLT) panels [10]. The authors noted convergence issues when implementing certain test conditions especially related to the load transfer device. The current study introduces and validates a FE model for glulam and CLT elements developed within the explicit LS-DYNA framework [12], focusing on the application of the built-in wood material model.

2 – LITERATURE REVIEW

Equivalent SDOF analysis is a widely used method for investigating the response of structural elements subjected to blast loading. This approach simplifies complex structural behaviour by representing a continuous structural element as an equivalent system with a defined resistance function, equivalent mass, and assumed deflected shapes [13]. The validity and applicability of the equivalent SDOF analysis method for predicting the

¹ Mehdi Saloo, PhD Candidate, Carleton University, Ottawa, Canada, mehdisaloo@cmail.carleton.ca

² Christian Viau, Assistant Professor, Carleton University, Ottawa, Canada, christian.viau@carleton.ca

³ Ghasan Doudak, Professor, University of Ottawa, Ottawa, Canada, gdoudak@uottawa.ca

response of mass-timber elements under blast loading have been extensively investigated [2-7, 14-15]. However, this modelling approach is limited to instances where a single failure mode governs, usually flexural, which may not fully capture the complex response of engineered wood elements.

Finite element analysis (FEA) is a widely used numerical technique for analysing structural members. To obtain reliable results, FEA requires the use of representative material properties, such as strength and elastic moduli, as well as failure criteria that captures all possible deformation and failure modes. The application of FEA in timber entails specific failure criteria capable of capturing wood's behaviour due to the inherent variability and directional differences in the properties of wood, which complicate the process of accurately determining material characteristics. Capturing wood's failure modes in FEA is further complicated by its anisotropic properties and the need to account for both brittle and ductile failure modes. Sandhaas et al. [16] developed a simplified constitutive model for wood based on continuum damage mechanics (CDM) to improve the numerical representation of wood behaviour under different loading conditions. The model accounts for the anisotropic nature of wood and the progressive damage mechanisms that influence its structural response. It incorporates elastic and inelastic deformation, stiffness degradation, and failure criteria. Oliveira et al. [10] investigated the behaviour of glulam and CLT using a constitutive material model incorporating the anisotropic nature of wood and high strain-rate effects via a user subroutine. The study highlighted the challenges of modelling wood, including its material variability due to natural defects (e.g., knots, fiber deviations), and complex failure interactions.

3 – FINITE ELEMENT MODEL

3.1 MODEL DEFINITION

The LS-DYNA FEA explicit solver was used to simulate and solve the time-dependent response of glulam and CLT members against shock-tube simulated far-field blast loads. LS-DYNA utilizes “keywords”, which are built-in input interface functions whereby variables and parameters are provided by the analyst, which are meant to simplify the modelling process without the need to work through backend codes. The LOAD_SEGMENT_SET keyword in LS-DYNA was used to simulate blast pressure. In this method, the recorded experimental blast pressure curve is defined using the DEFINE-CURVE keyword and directly applied to the shock-front surface. Previous studies [e.g., 17-21] have demonstrated that FEA modelling in LS-

DYNA can predict the blast behaviour of the structural elements with sufficient accuracy when the structural member is subjected to a far-field blast load.

Three dimensional first-order eight-node solid elements were used in all analyses and the mechanical behaviour of wood and its damage were modelled using the *Mat_143 (*Mat_Wood), which uses a reduced form of the Modified Hashin failure criteria [22]. The model uses six strength parameters derived from uniaxial and pure-shear testing to numerically quantify parallel and perpendicular to grain tensile and compression failures, as well as various shear failures. The model applies the analytical form of the Hashin criterion differently for parallel- and perpendicular-to-grain failure modes, as presented in Equations (1) and (2), respectively [22]. Failure occurs when f_{\parallel} and f_{\perp} are equal to or greater than zero. Element erosion was enabled in the model to account for parallel-to-grain damage and failure, whereby an element is automatically removed from the computational domain upon failure due to parallel-to-grain damage. This approach helps prevent numerical instabilities due to an element's extremely low stiffness and strength.

$$f_{\parallel} = \frac{\sigma_L^2}{X_{\parallel}^2} + \frac{(\sigma_{LT}^2 + \sigma_{LR}^2)}{S_{\parallel}^2} - 1 \quad X_{\parallel} = \begin{cases} X_T & \text{for } \sigma_L > 0 \\ X_C & \text{for } \sigma_L < 0 \end{cases} \quad (1)$$

$$f_{\perp} = \frac{(\sigma_R + \sigma_T)^2}{Y_{\perp}^2} + \frac{(\sigma_{RT}^2 - \sigma_R \sigma_T)}{S_{\perp}^2} - 1 \quad Y_{\perp} = \begin{cases} Y_T & \text{for } \sigma_R + \sigma_T > 0 \\ Y_C & \text{for } \sigma_R + \sigma_T < 0 \end{cases} \quad (2)$$

In the parallel-to-grain failure mode, X_T represents the tensile strength parallel to the grain, while X_C denotes the compressive strength parallel to the grain. In the perpendicular-to-grain failure mode, Y_T corresponds to the tensile strength perpendicular to the grain, and Y_C represents the compressive strength perpendicular to the grain. S_{\parallel} is the shear strength parallel to the grain, whereas S_{\perp} is the shear strength perpendicular to the grain. σ_L is the longitudinal (parallel-to-grain) stress, while σ_R is the radial (perpendicular-to-grain) stress, and σ_T is the tangential (perpendicular-to-grain) stress. σ_{LR} is the longitudinal-radial shear (parallel-to-grain) stress, σ_{LT} is the longitudinal-tangential shear (parallel-to-grain) stress, and σ_{RT} is the radial-tangential shear (perpendicular-to-grain) stress.

3.2 MODELLING INPUTS & EXPERIMENTAL TEST PROGRAM FOR VALIDATION

The FE models and modelling approach were validated using the test results from an experimental study that examined the behaviour of glulam and CLT structural

elements when subjected to simulated blast loads [8, 23]. Six experimentally tested specimens were selected for FE modelling of glulam and CLT elements in this study. All samples measured 2,500 mm in length and included 24f-ES grade glulam beams (86 mm × 178 mm) and E1 grade 5-ply CLT panels (445 mm × 175 mm). The shock tube uses pressurized air to produce uniform reflected pressures and impulses, simulating the effects of far-field blast explosions. A summary of the experimental testing of glulam and CLT specimens, including peak reflected pressure, reflected impulse, and failure modes, is presented in *Table 1*. Experimentally recorded pressures are established in the FEA environment and applied directly to the shock-front surface of the Load Transfer Device (LTD) to simulate the experimental conditions.

The FEA model was created to mirror the experimental specimens, boundary conditions, and loading configurations, and the anticipated results. In order to assess the predictive capability of the mode, the predicted displacements, resistances, and failure modes were compared to the experimental findings. The material model incorporates inputs derived from manufacturer specifications and literature. The values and sources of these properties are detailed in this section, with a summary of all inputs for the FEA model presented in *Table 2*. The density of the glulam and CLT specimens is calculated based on the mass and geometry of each specimen. The masses of the glulam and CLT specimens were determined to be 20.8 kg and 101.7 kg, respectively [8]. Notably, the suggested value for G_{TR} in the literature [10] was found to be incompatible with MAT-143 in LS-DYNA [12, 22], which requires that E_T be less than four times the magnitude of G_{TR} . Given that G_{TR} and E_T are not independent, the value of G_{TR} from the literature [10] was slightly increased to satisfy the MAT-143 requirement in LS-DYNA [12, 22]. The glulam beams were modelled as homogeneous members, while the CLT panels were constructed with distinct longitudinal and transverse laminates. A perfect bond between the layers of the CLT panel was assumed in the FEA environment. As shown in *Fig. 1*, other experimental components such as the LTD, which is used to convert the blast pressure into

two concentrated point loads, and the pinned boundary conditions, were also implemented into the model. The boundary supports were represented by four cylindrical rigid bodies acting as pinned supports to replicate the boundary conditions used in the full-scale experimental tests. The LTD, which weighs a total of 284 kg, was modelled as a rigid planar surface element and two load-transfer beams with rollers, with both LTD beams being rigidly connected to the LTD surface element to mimic in-situ conditions. A hard contact between the LTD and the specimen was used, whilst allowing for the LTD and specimen to detach during rebound. These modelling methodologies were used to minimize discrepancies between numerical and experimental test results.

Table 2: Material properties

Property	Glulam	CLT (Long./Trans.)	Ref.
Mass Density	543 kg/m ³	522 kg/m ³	[8]
E_L (Parallel-to-Grain Elastic Modulus)	13100 MPa	11700 / 9000 MPa	[10]
E_T (Perpendicular-to-Grain Elastic Modulus)	437 MPa	390 / 300 MPa	[10]
G_{LT} (Parallel shear modulus)	819 MPa	731 / 563 MPa	[10]
G_{TR} (Perpendicular shear modulus)	112 MPa	100 / 80 MPa	[12, 22]
ν_{LT} (Parallel major Poisson's ratio)	0.47	0.47	[10]
X_T (Parallel tensile strength)	33.7 MPa	27.7 / 5.8 MPa	[10]
X_C (Parallel compressive strength)	54.5 MPa	34.7 / 16.2 MPa	[10]
Y_T (Perpendicular tensile strength)	1.4 MPa	1.4 MPa	[10]
Y_C (Perpendicular compressive strength)	11.3 MPa	8 MPa	[10]
$S_{ }$ (Parallel shear strength)	10.9 MPa	10.9 MPa	[10]
S_{\perp} (Perpendicular shear strength)	27 MPa	27 MPa	[23]
$GF_{ }$ (Parallel fracture energy in tension)	6 N/mm	6 N/mm	[10]
$GF_{2 }$ (Parallel fracture energy in shear)	84 N/mm	84 N/mm	[22]
GF_{\perp} (Perpendicular fracture energy in tension)	0.4 N/mm	0.4 N/mm	[22]
$GF_{2\perp}$ (Perpendicular fracture energy in shear)	0.8 N/mm	0.8 N/mm	[22]

Table 1: Summary of Experimental Testing of Glulam and CLT Specimens [8, 10]

Test	P_r (kPa)	I_r (kPa-ms)	Observed Failure Mode
GL1.1	21.6	201.1	Flexural
GL2.1	30.9	289.9	Elastic
GL2.2	35.5	305.9	Flexural
CLT1.1	80.2	799.5	Rolling Shear then Flexural
CLT2.1	42.1	417.2	Elastic
CLT2.2	82.4	777.2	Rolling Shear then Flexural

In comparison, the numerical FE model developed by Oliveira et al. [10] did not explicitly include the LTD in the modelling environment due to issues with numerical instability. Instead, the inertial contribution of the LTD (284 kg) was accounted for by distributing its effective mass over the middle third of the member by increasing the material density in that region. While this approach provided sufficient numerical stability and good results, the comparison with experimental test results was limited to the maximum inbound displacement [10].

The current study utilized an element mesh size of 20 mm for the glulam specimens and 35 mm element mesh size was chosen for the CLT model since it provided an acceptable compromise between the accuracy of the results and computational efficiency.

4 – RESULTS AND DISCUSSION

The FE modelling results were evaluated based on the displacement-time history, resistance-displacement relationship, and overall observed damage. The displacement-time history was obtained from a mid-span node located on the tension side of the modelled specimens, while the reaction-time histories were recorded from the rigid pins in contact with the tension face at the supports. The numerical results are compared and discussed alongside the corresponding experimental test data in this section.

Table 3 summarizes the findings from both the experimental and numerical FE analysis, highlighting the peak resistance and the mid-span displacement observed at peak resistance. On average, the model overpredicted the peak resistance by 3.4% (COV = 12%) and underpredicted displacement at peak by 3.5% (COV = 11%), with maximum absolute errors of 20% and 15%, respectively. These ratios fall within the anticipated variability ranges, since the inputs were obtained from existing literature. Similarly, the numerical FE model developed by Oliveira et al. [24] slightly underpredicted the peak resistance by 4.3% (COV = 12%) and overpredicted the displacement at peak resistance by 10.6% (COV = 11%), indicating a comparable level of accuracy between the two approaches. Moreover, in both the current study and that by Oliveira et al. [24], the applied loads from the blast waves involved an idealization process, where the peak reflected pressures and impulses from experiments were transformed to an equivalent idealized triangular pressure-time history.

Representative experimental and numerical resistance curves are illustrated in Fig. 2 for specimens GL2.2 and

CLT1.1 [8,10]. The resistance curves obtained from the model matched reasonably well with the experimental resistance curves, as shown in Fig. 2. Unlike SDOF modelling, which requires the resistance curve as an input, FEA generates the resistance curve based on the material properties implemented by the analyst.

The overall numerical results for the resistance curves during pre-peak behaviour were consistent with the experimental test results for both glulam and CLT specimens, indicating that the model stiffness matched that of the experimental specimens. For CLT panels, the loss of the outermost longitudinal layers corresponded with peak resistance when flexural failure occurred, as observed in specimen CLT1.1 (see Fig. 2b). No significant post-peak behaviour was noted for the glulam specimens in both the experimental and numerical results, as shown in Fig. 2a. In contrast, the CLT specimens demonstrated some post-peak capacity, as shown in Fig. 2b.

Table 4 summarizes the observed behaviour in the glulam and CLT specimens through experimental testing and FE modelling. The results indicate that FEA modelling can predict the peak resistance and inbound displacement exhibited by glulam and CLT specimens, except for specimen GL1.1, which remained in the elastic region, and specimen GL2.1, which experienced flexural failure in the FE modelling environment.

This minor discrepancy can be explained by the fact that average design parameter values were used as inputs. In the case of GL1.1, for example, this specimen may have been weaker than anticipated based on the parameters used as input into the LS-DYNA model, leading to an underprediction of damage. This behaviour was also observed by Oliveira et al. [10], suggesting that the discrepancy may be attributed to inherent material variability rather than limitations of a specific modelling approach.

Table 3: Summary of Numerical and Experimental Results

Test	Peak Resistance (kN)			Displacement at Peak (mm)		
	Exp.	Num.	Err. (%)	Exp.	Num.	Err. (%)
	[24]			[24]		
GL1.1	54.4	65.2	+20	26.2	28.9	+10
GL2.1	76.7	67.5	-12	32.6	29.6	-9
GL2.2	78.6	71	-10	33.7	36.5	+8
CLT1.1	186.5	207	+11	32.9	32.5	-1
CLT2.1	125.8	133	+6	21.5	18.4	-14
CLT2.2	180.6	191	+6	33.5	28.5	-15

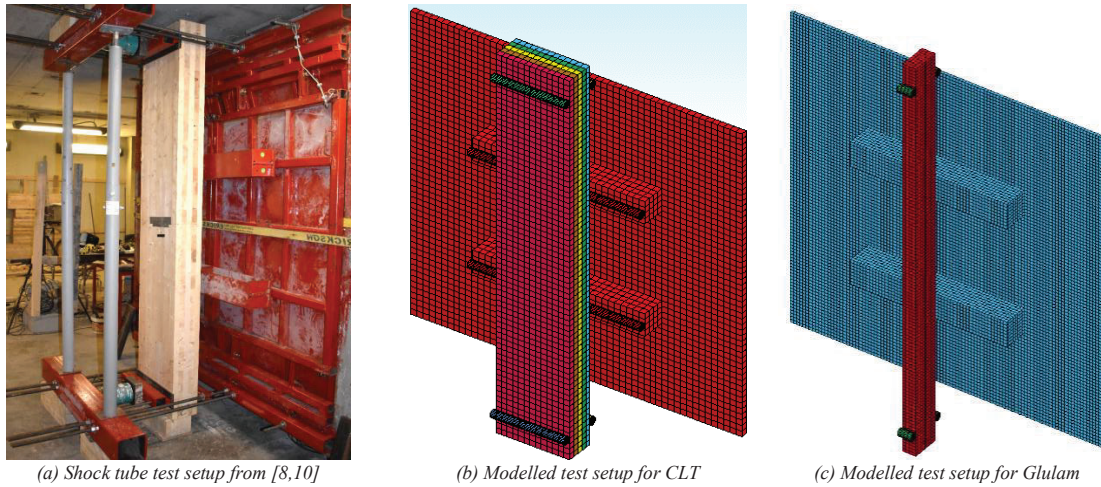
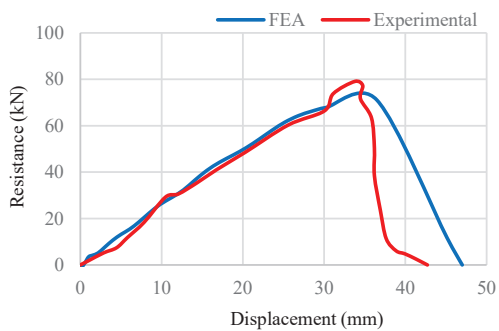
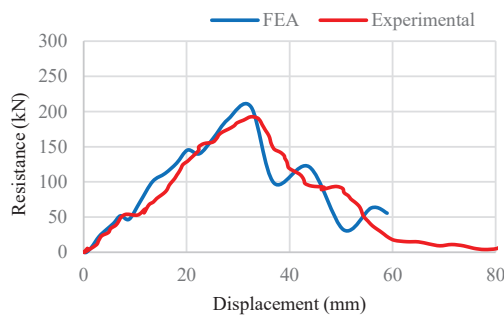


Figure 1. Testing and modelling of CLT and glulam specimens subjected to shock tube testing



(a) Glulam (GL2.2)



(b) CLT (CLT1.1)

Figure 2. Representative Experimental [8,10] and numerically-predicted resistance curves

While specimen GL2.1 exhibited minor flexural damage, this did not significantly affect the overall structural behaviour, and the specimen was able to return to its original position. The failure was localized and occurred at a region outside the beam mid-span [8,10,24]. In all the modelled glulam specimens, including the modelled

GL2.1 specimen, failure was consistently initiated in the outer layer on the tension side near mid-span, where maximum flexural stress occurs, corresponding to initial element deletion and damage propagation through the cross-section. However, the results presented in *Table 3* show comparable FEA results regarding the peak resistance and the mid-span displacement observed at peak resistance. These results indicate that while there are variances in terms of the specific location of damage initiation and propagation, a reasonable prediction of the overall behaviour at the structural rather than material level can be achieved using the described modelling methodology.

As shown in *Fig. 3*, while the general “shape” of the crack propagation differs between the experimental results and the current study’s models, the extent of the predicted damage closely aligns with the experimental test results. Experimentally, the cracks in GL2.2 (see *Fig. 3a*) began at mid-span and propagated rapidly, resulting in a flexural failure characterized by diagonal cracks spreading through the majority of the cross-section [8,10]. As shown in *Fig. 3b*, where flexural failure is initiated at the mid-span, the extent of damage occurring in the modelled glulam specimens aligns closely with the findings of a similar study [10], where failure consistently initiated in the outer laminate on the tension side near mid-span, followed by progressive damage propagation through the cross-section. This agreement suggests that, while the current study and that by Oliveira et al. [10] are based on different modelling assumptions and failure criteria, both models capture the fundamental failure mechanisms of glulam beams under simulated far-field blast loads.

Similar to numerical results for glulam elements, the CLT numerical model captured the overall failure mode of CLT specimens with reasonable accuracy, whereby failure initiation can be seen as occurring near the mid-

Table 4: Behaviour of Glulam and CLT Specimens Observed during Experimental Testing [10] and FE Modelling

Test	Experimentally Observed Behaviour	FEA-Predicted Behaviour
GL1.1	Flexural	Elastic
GL2.1	Elastic	Flexural
GL2.2	Flexural	Flexural
CLT1.1	Rolling Shear then Flexural	Flexural
CLT2.1	Elastic	Elastic
CLT2.2	Rolling Shear then Flexural	Flexural



Figure 3. Representative results for glulam (GL2.2)

span of the panel, as shown in Fig. 4. The FE models were found to accurately predict the initial stiffness and peak resistance, as well as the extent of failure within the longitudinal layers, leading to an overall flexural failure of the CLT panel. These results indicate that while adjustments of the strength values to calibrate model to be more attuned to the specific effects of weak areas in the investigated timber elements can lead to further alignment of resistance behaviour of the FE model and

experimental results, the overall flexural failure mode of specimens (Fig. 2, Fig. 3, and Fig. 4) can be well captured. However, further refinements are needed to accurately capture the extent of damage as well as capture other potential failure modes.



Figure 4. Representative results for CLT (CLT1.1)

5 – CONCLUSIONS

Key findings from a numerical study investigating the behaviour of heavy timber elements subjected to far-field blast loads were presented and discussed. Model validation was conducted for both glulam and CLT specimens subjected to shock-tube simulated far-field blast loads. The metrics used in this comparison include the mid-span displacement-time history, dynamic resistance curve, and overall failure modes. The results of this study showed that the FE model can predict the behaviour of timber members with reasonable accuracy in terms of failure mode, mid-span displacement, and resistance curve. These findings highlight a significant advantage in using FEA over simplified modelling methods, such as SDOF modelling. Furthermore, the use of design parameters from engineered wood manufacturers and design standards as inputs into the

material model provide adequate accuracy to produce realistic predictions of the overall behaviour of heavy and mass timber elements subjected to far-field blast loads. The validated model can be used to generate resistance curves of glulam and CLT members, as well as predict the behaviour of timber members subjected to far-field blast loads, offering a cost-effective alternative to experimental testing.

6 – REFERENCES

- [1] G. Doudak, C. Viau, and D.N. Lacroix. "Proposed design methods for timber members subjected to blast loads." *Journal of Performance of Constructed Facilities* 36.3 (2022): 04022020.
- [2] D.N. Lacroix and G. Doudak. "Determining the dynamic increase factor for glued-laminated timber beams." *Journal of Structural Engineering* 144.9 (2018): 04018160.
- [3] M. Poulin, C. Viau, D. N. Lacroix, and G. Doudak. "Experimental and analytical investigation of cross-laminated timber panels subjected to out-of-plane blast loads." *Journal of Structural Engineering* 144, no. 2 (2018): 04017197.
- [4] C. Viau and G. Doudak. "Investigating the behavior of light-frame wood stud walls subjected to severe blast loading." *Journal of Structural Engineering* 142.12 (2016): 04016138.
- [5] C. Viau and G. Doudak. "Behavior and modeling of glulam beams with bolted connections subjected to shock tube-simulated blast loads." *Journal of Structural Engineering* 147, no. 1 (2021): 04020305.
- [6] D.N. Lacroix and G. Doudak. "Investigation of dynamic increase factors in light-frame wood stud walls subjected to out-of-plane blast loading." *Journal of Structural Engineering* 141.6 (2015): 04014159.
- [7] D. Lacroix, C. Viau, E. Battelli, and G. Doudak. "Enhancing the performance of light-frame wood studs using glass fibre-reinforced polymers." *Engineering Structures* 245 (2021): 112973.
- [8] D. Oliveira, C. Viau, and G. Doudak. "Behaviour of mass timber members subjected to consecutive blast loads." *International Journal of Impact Engineering* 173 (2023): 104454.
- [9] CSA. "Design and assessment of buildings subjected to blast loads in CSA S850." Canadian Standards Association, CSA Group: Mississauga, ON, 2023.
- [10] D. Oliveira, C. Viau, and G. Doudak. "Modelling the behaviour of heavy and mass timber members subjected to blast loads." *Engineering Structures* 291 (2023): 116397.
- [11] D.S.S. Corp Abaqus Unified FEA 6.14-2 ed. USA2014. Providence, RI.
- [12] ANSYS Inc., ANSYS LS-DYNA Solver (LS-Run) 2023 R1, PA, USA: ANSYS Inc., 2023.
- [13] J.M. Biggs. "Introduction to Structural Dynamics." New York, NY: McGraw-Hill, 1964.
- [14] D.N. Lacroix and G. Doudak. "Towards enhancing the post-peak performance of glued-laminated timber beams using multi-directional fibre reinforced polymers." *Engineering Structures* 215 (2020): 110680.
- [15] D.N. Lacroix and G. Doudak. "Effects of high strain rates on the response of glulam beams and columns." *Journal of Structural Engineering* 144.5 (2018): 04018029.
- [16] C. Sandhaas, J.W.G.V.D. Kuilen, and H.J. Blass. "Constitutive model for wood based on continuum damage mechanics." *World Conference on Timber Engineering*, 2012.
- [17] M. Saloo, M. Z. Kabir, and M. R. Khedmati. "Assessment of performance criteria of reinforced concrete beams retrofitted with FRP fabrics subjected to extreme impulsive loading." *Advanced Composite Materials* 30.1 (2021): 1-23.
- [18] R. P. Bohara, S. Linforth, A. Ghazlan, T. Nguyen, A. Remennkov, and T. Ngo. "Performance of an auxetic honeycomb-core sandwich panel under close-in and far-field detonations of high explosive." *Composite Structures* 280 (2022): 114907.
- [19] Q. Su and X. Zhai. "Dynamic response of single-layer reticulated shell with explosion-protection wall under blast loading." *Thin-Walled Structures* 127 (2018): 389-401.
- [20] R. Zhang, J. Jia, H. Wang and Y. Guan. "Shock response analysis of a large LNG storage tank under blast loads." *KSCE Journal of Civil Engineering* 22 (2018): 3419-3429.

[21] C. Kyei and A. Braimah. "Effects of transverse reinforcement spacing on the response of reinforced concrete columns subjected to blast loading." *Engineering Structures* 142 (2017): 148-164.

[22] Y. D. Murray. "Manual for LS-DYNA wood material model 143." No. FHWA-HRT-04-097. United States. Federal Highway Administration, 2007.

[23] E. J. Kramer, M. C. Flemings, R. W. Cahn, S. Mahajan, K.J. Buschow, and B. Ilshner. [Encyclopedia] "Encyclopedia of Materials - Science and Technology." Volumes 1-11. Elsevier, 2001.

[24] D. Oliveira, C. Viau, and G. Doudak. "Predictive Capabilities of Finite Element Modelling for Timber Members Subjected to Blast Loads." *World Conference on Timber Engineering*, 2023.